Electrochemical hydrogen storage behaviors of nanostructured $La_{1-x}Sr_xCoO_3$ (x = 0-1.0) prepared by sol-gel method

Peng Yan[1,a], Yanyan Bao[2], Chunyu Qiao[1], Dianxue Cao[2] and Guiling Wang[2]

[1]*College of Material and chemical Engineering, Heilongjiang Institute of Technology Harbin, 150050, P R China*
[2]*Laboratory of Superlight Material and Surface Technology of Ministry of Education, College of Material Science and Chemical Engineering, Harbin Engineering University, Harbin, 150001, P R China*

Abstract. The $La_{1-x}Sr_xCoO_3$ perovskite oxides were synthesized by a sol-gel method, the electrochemical properties of them were studied as negative electrodes for nickel–metal hydride batteries in aqueous KOH solution. The results show that the electrode with the Sr content of x = 1.0 shows the best performance among the as-prepared materials, whose maximum discharge capacity is 103.5 mAh g^{-1} and the capacity remains 100 mAh g^{-1} after 20 cycles at the discharge current density 100 mA g^{-1}, the retention rate is 97.1%. The possible existence of strong chemisorption of hydrogen may lead to the lower discharge capacity of nanoparticles according to CV results. Analysis of electrode reaction mechanism demonstrates that the discharge capacity is attributed to the valence change of Co ions, so the electrocatalytic activity can be enhanced by A site metal substitution.
Keywords: strontium substitution; perovskite; electrochemical properties.

1 Introduction

Hydrogen is considered to be an ideal energy carrier. However, hydrogen storage with a safe and cheap system is crucial for hydrogen fuel cells or hydrogen-driven combustion engines [1]. A variety of alloys have been investigated as hydrogen storage material, including AB_5-type rare-earth metal alloys [2], AB_2-type Laves phase alloys [3], AB-type intermetallic compounds [4], Mg-based alloys [5], alloy nanoparticles [6] and some transition metal–metalloid alloys, such as (Co-B, Co-S , and Co-Si alloys [7-10]). Among these alloys, the AB_5-type rare-earth metal alloys are widely used in commercial batteries because of their suitable plateau pressure and fast activation. However, their discharge capacities are comparatively low, the reversible capacities are only about 300 mAh g^{-1}. Therefore, on the one hand, great efforts, such as the optimization of the alloy compositions and the surface modifications, have been undertaken to improve the electrochemical capacity and the high rate capability of these materials. On the other hand, many new hydrogen storage materials have been synthesized, with improved electrochemical properties at lower cost than state-of-the-art materials [11, 12].

Several new types of materials for electrochemical hydrogen storage have been investigated, including: (1) the sixth main group metal compounds, oxides such as CuO nanoribbon arrays [13],

[a] Corresponding author : 22382023@qq.com

manganese oxides [14], sulfides such as Fe_3S_4 [15], MoS_2 [16], TiS_2 [17], Bi_2S_3 [18], Ni_3S_2 [19], selenides such as 3D rose-like Bi_2Se_3 hierarchitectures [20], Sb_2Se_3 nanowires [21]; (2) carbon material and its modification complexes [22-26]; (3) some special structure nanomaterials, BN nanotubes [27], BiOI hierarchical structures [28], $Cu(OH)_2$ nanoribbon arrays [29], ultra-long t-Se submicrotubes [30]. These materials can be used as new negative electrode materials for nickel–metal hydride (Ni-MH) batteries with higher discharge capacity than that of the traditional materials. Mandal et al. [31] had developed an unprecedented intake of hydrogen by $BaMnO_3$/Pt to the extent of 1.25 mass% at moderate temperatures (190-260ºC) at ambient pressure. However, little attention has been paid to the study of proton-conductive perovskite-type oxides despite their promising characteristics as negative electrode materials for Ni/MH secondary batteries. Esaka et al. [32] had proposed perovskite-type oxides $ACe_{1-x}M_xO_{3-\delta}$ (A = Sr or Ba, M = rare earth element) prepared by a conventional solid-state reaction method as innovative electrode materials for Ni/MH batteries. ABO_3-type perovskite oxides are superior to traditional hydrogen storage alloys because of their high theoretical hydrogen storage capacity and at low cost. However, further research results have not been extensively reported.

In this work, perovskite $La_{1-x}Sr_xCoO_3$ (x = 0-1.0) was prepared by a sol-gel method, and its electrochemical hydrogen storage properties were investigated. The effects of Sr substitution on the overall electrochemical properties of nanoparticles and the electrochemical hydrogen storage mechanism were investigated, respectively.

2 Experimental

2.1 Preparation and structural characterization

$La_{1-x}Sr_xCoO_3$ (x = 0-1.0) perovskite oxides were synthesized by a sol–gel method using $La(NO_3)_3 \cdot 6H_2O$, $Sr(NO_3)_2$ and $Co(NO_3)_3$ as source materials and chitosan as the gelling agent. Details of $La_{1-x}Sr_xCoO_3$ oxides synthesis can be found elsewhere [33]. Stoichiometric amounts of nitrates were dissolved in a small amount of distilled water to get A solution. Certain amount of chitosan (metal/ chitosan molar ratio = 1/1) was dissolved in 2 vol% acetum solution to get B solution. The A solution was added dropwise to the B solution under constant stirring at 80-90ºC, where polymerization occured in the liquid solution and led to a homogeneous sol. When the sol was further heated to remove the excess of solvent, an intermediate gel was formed. Drying the gel at 100ºC in air was performed before sintering at 650ºC for 5 h in muffle furnace to form $La_{1-x}Sr_xCoO_3$ (x = 0-1.0).

Structures of the perovskite samples were analyzed using X-ray diffractometer (Rigaku TTR III) with Cu K_α radiation (λ = 0.1514178 nm). The 2θ ranges from 10° to 90° with a scan rate of 5º min^{-1} and a step width of 0.01º. The morphology was examined by a scanning electron microscope (SEM, JEOL JSM-6480).

2.2 Electrochemical measurements

Negative electrodes were fabricated by mixing as-prepared materials with conducting Ni powders, an organic polytetrafluroethylene (PTFE) and sodium carboxymethylcellulose (CMC) in a weight ratio of 2:6:1:1 (LSCO: Ni: PTFE: CMC). The powder mixture was pasted into the substrate of nickel foam and pressed under 10 MPa pressure. Galvanostatic charge/discharge test was conducted in a three-compartment cell using a Land battery test instrument. A $Ni(OH)_2$/NiOOH electrode and a saturated calomel electrode (SCE) were used as the counter electrode and the reference electrode respectively. In each charge–discharge cycle test, the negative electrode was charged for 3 h at 100 mA g^{-1} and discharged at 30, 60, 100, 150 mA g^{-1} up to the cut-off voltage of -0.7 V. The electrolyte solution is 6 mol dm^{-3} KOH aqueous solution. The testing time between charge and discharge was 5 min. A computerized VMP3/Z potentiostat (Biologic) controlled by the EC-lab software was used for electrochemical measurements. All the tests were performed at room temperature.

3 Results and discussion

3.1 Material characterization

XRD patterns for the heat treated $La_{1-x}Sr_xCoO_3$ (x = 0-1.0) powders are shown in Fig. 1. All samples were heat treated at 650 °C for 5 h and fully developed into the single perovskite structure. All the diffraction peaks of pure $LaCoO_3$ sample match well with the standard XRD pattern of perovskite $LaCoO_3$ (JCPDS card No. 75-0279). The peaks at 29° 31°, 44° and 57° correspond to the reflections of $SrCoO_3$. With increasing Sr content (x > 0.2), the resultant powders are observed to have a tiny impure phase with characteristic peaks at 2θ = 25.1°, 36.7°, 44.3°, 50.2°. These peaks can be attributed to $SrCO_3$, which likely result from the reaction of strontium with CO_2 (from the combustion of Chitosan) during the annealing process. The peaks intensity grows with the strontium doping. No peaks from impurities such as cobalt oxides, lanthanum oxides and strontium oxides are observed. By the Scherrer equation from the XRD patterns, the particle sizes of the six samples are about 15-20 nm.

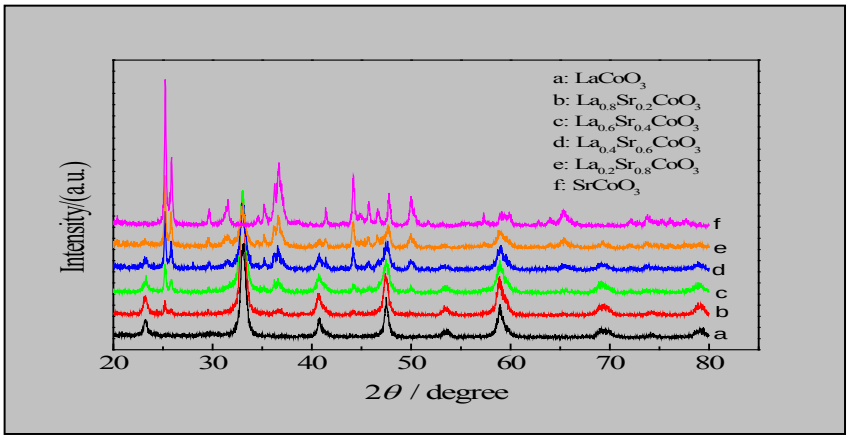

Figure 1. The XRD patterns of La1-xSrxCoO3 (x = 0-1.0).

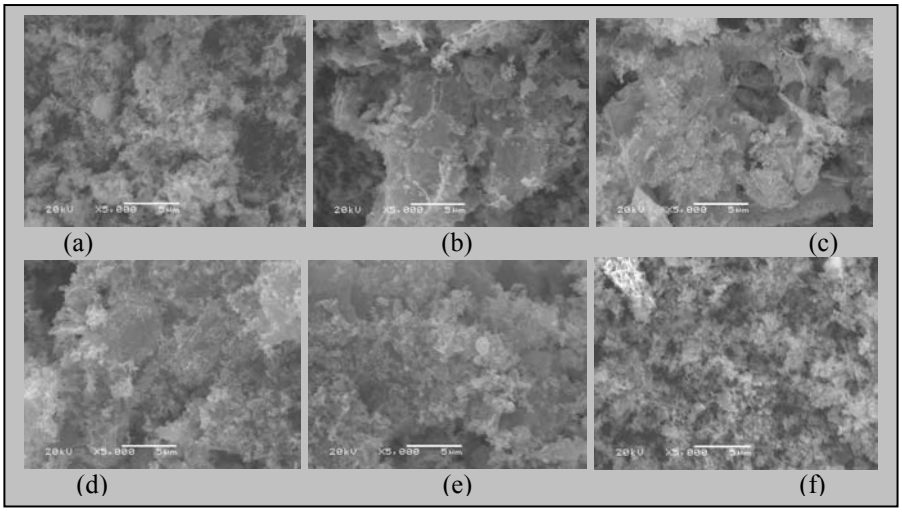

Figure 2. SEM images of La1-xSrxCoO3 (x = 0-1.0).

Fig. 2 shows the SEM patterns of a series of perovskite-type oxides $La_{1-x}Sr_xCoO_3$ (x = 0-1.0) calcined at 650 °C for 5 hours under air for various strontium ratios. These samples are composed of spheroidal, agglomerated particles of 15-20 nm. Further, average particle diameter decreases with

increasing strontium ratio. The aggregation is gradually obvious with the increasing contents of strontium substitution, while the best powder morphology is found in $SrCoO_3$ sample in which case the particles are uniform and well dispersed. This study indicates that all the powders have large numbers of nano pores and inhomogeneous pore distribution.

3.2 Electrochemical performance

Fig.3 displays the discharge capacity varying with cycle number for the $La_{1-x}Sr_xCoO_3$ (x = 0-1.0) electrodes at the discharge current density of 100 mA g^{-1}. The $LaCoO_3$ electrode has the relatively high initial discharge capacity of 92.9 mAh g^{-1}, but the discharge capacity decreases distinctly, up to 57.5 mAh g^{-1} at the 20th cycle. When the Sr content is 0.2, the initial discharge capacity is 86.8 mAh g^{-1}, from the 4th cycle to the 20th cycle, the discharge capacity keeps steady about 80.2 mAh g^{-1}, which is higher than $LaCoO_3$ electrode, so Sr substitution improves the cycle performance. The electrode with strontium content of x = 0.4 is similar to the electrode (x = 0.2), but has a poorer discharge capacity. The electrode (x = 0.6) needs several cycles to activate, it has the lower initial discharge capacity of 78.4 mAh g^{-1}, and in the 20th cycle, the discharge capacity increases gradually to 88.6 mAh g^{-1}. The electrode (x = 0.8) needs four cycles to activate and then the discharge capacity keeps steady about 66.5 mAh g^{-1}. Obviously, it can be seen that $SrCoO_3$ electrode shows very well cycle stability, the discharge capacity can reach 103.5 mAh g^{-1}, the capacity retention is 97.1% in the 20th cycle. The discharge capacity can be enhanced, for example, by modifying the $SrCoO_3$ powder structure to improve the electrochemical reaction of hydrogen within the electrode.

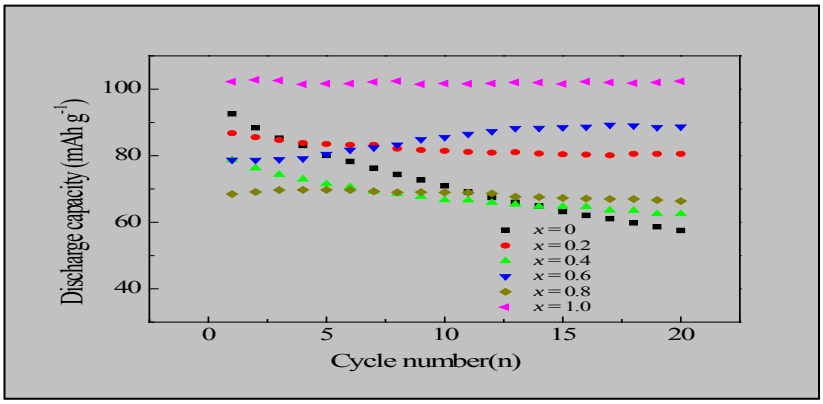

Figure 3. Cycle stability of La1-xSr_xCoO_3 (x = 0-1.0) electrodes at current density of 100 mA g^{-1}.

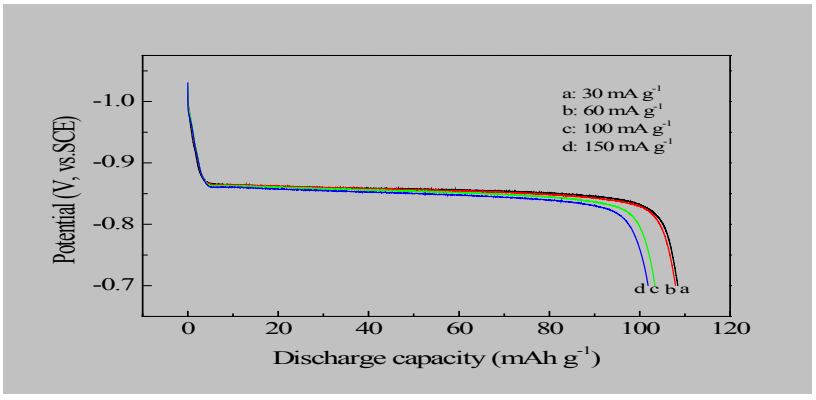

Figure 4. Discharge curves of $SrCoO_3$ electrode at different current densities.

Fig. 4 shows the discharge performance of the $SrCoO_3$ electrode at the discharge current density of 30, 60, 100, 150 mA g^{-1}. The electrode presents a long and flat discharge plateau, showing the highest discharge capacity of 108.6 mAh g^{-1} at a current density of 30 mA g^{-1} at room temperature. Theflat discharge plateaus appear around −0.85 V at different discharge current densities, which are similar to those of the typical AB_5-type alloys [8]. Therefore, it is reasonable to attribute the discharge process to the dehydrogenation process. It is obvious that the reversible discharge capacity goes lower when the current density becomes higher. It is recognized that high discharging current density has negative effects on electrodes such as increasing the separation speed of the oxides from Ni foam, so the result is consistent with the traditional view.

The kinetic properties of the $SrCoO_3$ electrodes were investigated by measuring the rate capability and cycling ability at different discharge current densities. Fig.5 shows the cycle life of the $SrCoO_3$ electrode at the discharge current density of 30, 100, 150 mA g^{-1}. It is obvious that the reversible discharge capacity goes lower when the current density becomes higher. However, something worthy to note is that the cycle life of the electrode is not affected. The main reason on this phenomenon is possibly that when the current density is high, a passivation layer forms on the surface of the oxides, by which further powder off is prevented.

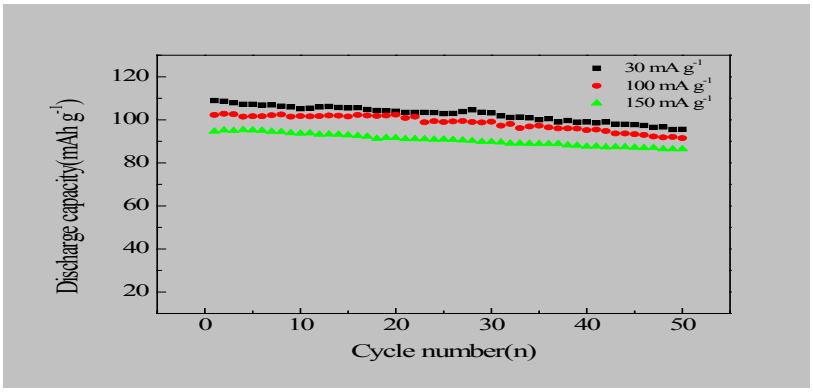

Figure 5. Cycle performance of the $SrCoO_3$ electrode at different current densities.

Cyclic voltammogram (CV) was carried out to further test the electrochemical hydrogen adsorption-oxidation reactions of $SrCoO_3$ electrode in 6 mol dm^{-3} KOH solution. As shown in Figure 6, the anodic oxidation peak of hydrogen in the CV is in the potential range between -0.63 and -0.73 V, which is frequently observed for the electrochemical hydrogen storage electrodes. The cathodic adsorption peak of hydrogen is observed around -1.0 V, which is very similar to the CV feature for electrochemical reduction of H_2O in the potential position and peak shape. The desorption peak of hydrogen appears around -0.8 V in the anodic process, indicating a slow desorption process of hydrogen at $SrCoO_3$ electrode. Clearly, the desorption peak of hydrogen appears prior to the electrochemical oxidation peak of hydrogen, suggesting the possible existence of the strong chemisorption of hydrogen [27]. The mechanism of the electrochemical hydrogen storage process can be summarized as follows:

$$SrCoO_3 + H_2O + e^- = SrCoO_3 - H_{ads} + OH^- \quad (1)$$

$$SrCoO_3 - H_{ads} = SrCoO_3 - H_{ads} \quad (2)$$

$$2SrCoO_3 - H_{ads} = 2SrCoO_3 + H_2 \quad (3)$$

$SrCoO_3$–H_{ads} and $SrCoO_3$–H_{abs} are denoted as adsorbed hydrogen and absorbed hydrogen on $SrCoO_3$ nanoparticles, respectively. Hydrogen desorption from the Pd alloy electrode takes place in two mechanisms, electrochemical oxidation and nonelectrochemical recombination [34]. However, in alkaline solution hydrogen desorption by nonelectrochemical recombination is seldom observed in

electrodes with high electrocatalytic activity, where electrochemical oxidation process is dominant. The strong hydrogen desorption of nonelectrochemical recombination without charge transfer may occur at $SrCoO_3$ electrode, which leads to a low discharge capacity. The improvement of the electrocatalytic activity by surface modification with metals or alloys is expected to enhance the electrochemical hydrogen storage capacity of oxides electrode.

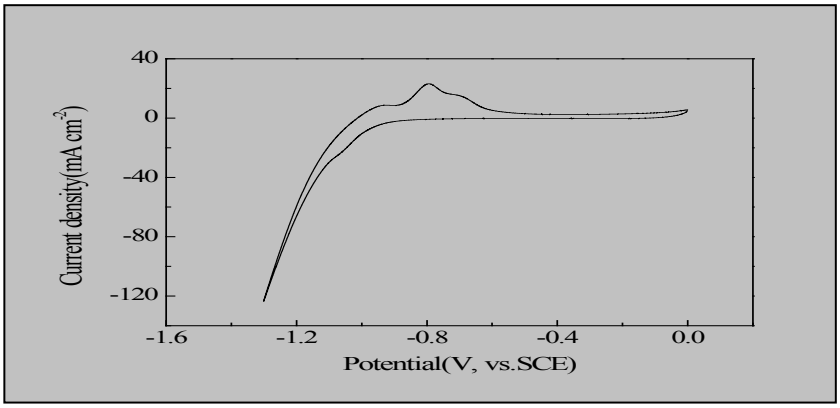

Figure 6. CV curve of $SrCoO_3$ electrode in 6 mol dm^{-3} KOH solution. Sweep rate, 10 mV s^{-1}.

In order to examine which attributed to the discharge capacity, we studied the discharge performance of pure Ni electrode for comparison. Fig.7 shows the discharge curves for the two electrodes at the discharge current density of 30 mA g^{-1}. It can be seen that pure Ni powder electrode shows a very low discharge capacity, only 2.6 mAh g^{-1}. We can infer that the high discharge capacity is mainly attributed by the electrochemical hydrogen storage of $SrCoO_3$ oxides. Nickel inclusions play a role of catalyst in charge-discharge process, which can catalyze the reduction of H_2O and adsorption of hydrogen on the electrode surface.

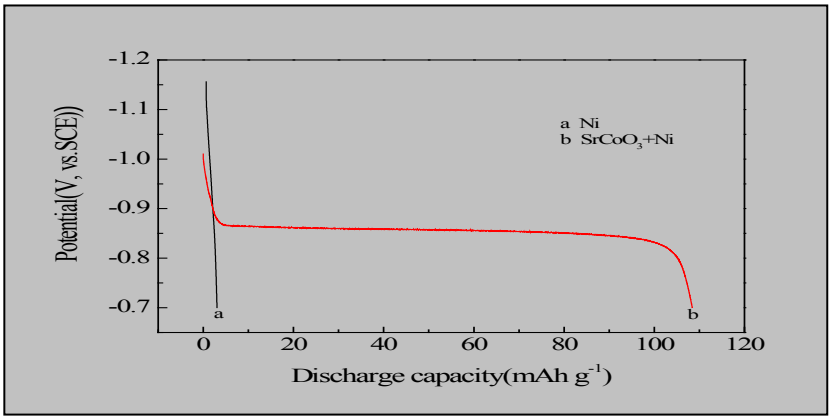

Figure 7. Discharge curves of Ni and $SrCoO_3$–Ni electrodes at current density of 30 mA g^{-1}.

In order to check the role of metal ions in the oxides, we measured the discharge property of $LaCoO_3$, $LaMnO_3$ and $SrCoO_3$ electrodes with Ni powder as additives at the discharge current density of 150 mA g^{-1}. As shown in Fig. 8, the discharge performance of $LaMnO_3$ electrode obviously falls off; no apparent discharge platform is observed. However, the discharge capacity of $LaCoO_3$ electrode reaches 84.8 mAh g^{-1}, which was much larger than $LaMnO_3$ electrode. From the comparison above, we can conclude that CoO_2 itself can adsorb and desorb some hydrogen but MnO_2 can storage relatively little hydrogen in the similar experiment. Cobalt is preferable to manganese at the B site in the perovskite-type structure (ABO_3). The curve of $SrCoO_3$ electrodes is similar to the $LaCoO_3$ electrodes, also the discharge capacity of them are more or less the same, indicating that they possess

similar electrochemical hydrogen storage performance. So, it is concluded that cobalt at the B site plays an important role in the hydrogen storage capacity of the electrodes. Electrochemical hydrogen storage is considered to be probably due to the valence change at the B site in the perovskite-type oxides.

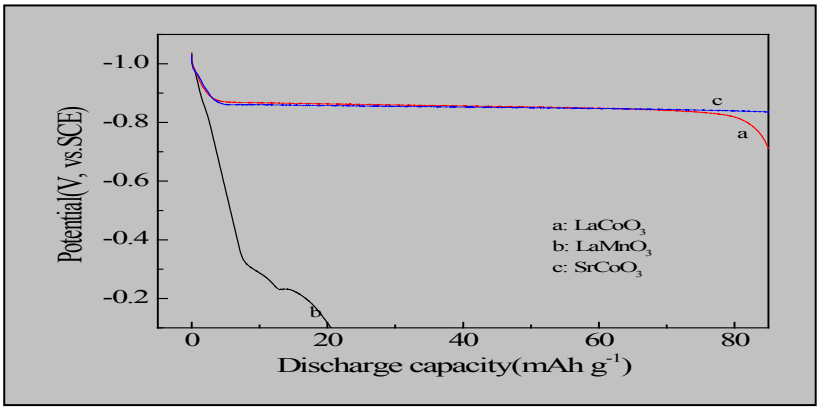

Figure 8. Discharge curves of $LaCoO_3$, $LaMnO_3$ and $SrCoO_3$ electrodes at current density of 150 mA g^{-1}

4 Conclusions

Perovskite-type oxides $La_{1-x}Sr_xCoO_3$ (x = 0-1.0) were synthesized by a sol-gel method using chitosan as a precursor. It is found that the obtained oxides are of perovskite structure with spheroidal, agglomerated particles of 15-20 nm. The results reveal that the series materials are suitable for hydrogen storage, with the highest discharge capacity of 103.5 mAh g^{-1} (when x = 1) at 100 mA g^{-1}, remaining 100 mAh g^{-1} after 20 cycles. The kinetic properties of the $SrCoO_3$ oxides were examined at different current densities and showed satisfying results. The hydrogen storage mechanism of $SrCoO_3$ electrode was also investigated. The element at the B site plays an important role in the hydrogen storage capacity. The $SrCoO_3$ electrode shows the preferable properties, which is a promising candidate as negative electrode material for Ni/MH batteries.

Acknowledgements

We gratefully acknowledge the financial support of this research by the Youth Science Foundation of Heilongjiang Institute (2013QJ12) and National Nature Science Foundation of China (51572052).

References

1. Schlapbach L, Züttel A, Nature, **414**, 353-358 (2001)
2. Wang Y, Zhao M, Li S, Wang L, Electrochim Acta, **53**,7831-7837 (2008)
3. Zhu YF, Pan HG, Gao MX, Ma JX, Li SQ, Wang QD, Int J Hydrogen Energy, **27**, 287-293 (2002)
4. Chiang CH, Chin ZH, Perng TP, J Alloys Compds, **307**, 259-265 (2000)
5. He G, Jiao L-F, Yuan H-T, Zhang Y-Y, Wang Y-J, J Alloys Compd, **450**, 375-379 (2008)
6. Tanaka K, Sowa M, Kita Y, Kubota T, Tanaka N, J Alloys Compd, **330-332**, 732-737 (2002)
7. Liu Y, Wang Y, Xiao L, Song D, Jiao L, Yuan H, Electrochem Commun, **9**, 925-929 (2007)
8. Qinghong Wang , Lifang Jiao , Hongmei Du. Int J Hydrogen Energy, **35**, 8357-8362 (2010)
9. Wang Y, Lee JM, Wang X, Int J Hydrogen Energy, **35**, 1669-1673 (2010)
10. Zhang Y, Jiao L, Wang Y, Wang Q, Zhang Y, Liu L, Yuan H, Int J Hydrogen Energy, **33**, 4819-4823 (2008)
11. Chen P, Xiong Z, Luo J, Lin J, Tan KL, Nature,**420**, 302-304 (2002)
12. Seayad AM, Antonelli DM, Adv Mater **16**, 765-777 (2004)

13. Gao P, Chen Y, Lv H, Li X, Wang Y, Zhang Q, Int J Hydrogen Energy, **34**, 3065-3069 (2009)
14. Men H, Gao P, Sun Y, Chen Y, Wang X, Wang L, Int J Hydrogen Energy, **35**,9021-9026 (2010)
15. Cao F, Hu W, Zhou L, Shi W, Song S, Lei Y, Wang S, Zhang H, *Dalton Transactions* 9246-9252 (2009)
16. Ye L, Wu C, Guo W, Xie Y, Chem Commun 4738-4740 (2006)
17. Chen J, Li S-L, Tao Z-L, Shen Y-T, Cui C-X, J Am Chem Soc, **125**, 5284-5285 (2003)
18. Li L, Sun N, Huang Y, Qin Y, Zhao N, Gao J, Li M, Zhou H, Qi L, Adv Funct Mater, **18**, 1194-1201 (2008)
19. Zhang B, Ye X, Dai W, Hou W, Xie Y, Chem Eur J, **12**, 2337-2342 (2006)
20. Sun Z, Liufu S, Chen X, Chen L, Chem Commun, **246**,3101-3103 (2010)
21. Jin R, Chen G, Wang Q, Sun J, Wang Y, J Mater Chem, **21**, 6628-6635 (2011)
22. Reyhani A, Mortazavi SZ, Mirershadi S, Moshfegh AZ, Parvin P, Golikand AN, J Phys Chem C **115**, 6994-7001 (2011)
23. Liu N, Yin L, Wang C, Zhang L, Lun N, Wang C, Qi Y, J Phys Chem C,**114**,22012-22018 (2010)
24. Reyhani A, Mortazavi SZ, Moshfegh AZ, Nozad Golikand A, Int J Hydrogen Energy, **35**,231-237 (2010)
25. Liu N, Yin L, Kang L, Zhao X, Wang C, Zhang L, Xiang D, Gao R, Qi Y, Lun N, Int J Hydrogen Energy, **35**,12410-12420 (2010)
26. Liu E, Wang J, Li J, Shi C, He C, Du X, Zhao N, Int J Hydrogen Energy **36**, 6739-6743 (2011)
27. Chen X, Gao XP, Zhang H, Zhou Z, Hu WK, Pan GL, Zhu HY, Yan TY, Song DY, J Phys Chem B, **109**, 11525-11529 (2005)
28. Lei Y, Wang G, Song S, Fan W, Pang M, Tang J, Zhang H, Dalton Trans, **39**, 3273-3278 (2010)
29. Gao P, Zhang M, Niu Z, Xiao Q, Chem Commun 5197-5199 (2007)
30. Zhang B, Dai W, Ye X, Hou W, Xie Y, J Phys Chem B **109**, 22830-22835 (2005)
31. Mandal TK, Sebastian L, Gopalakrishnan J, Abrams L, Goodenough JB, Mater Res Bull, **39**, 2257-2264 (2004)
32. Esaka T, Sakaguchi H, Kobayashi S, Solid State Ionics, **166**, 351-357 (2004)
33. Wang G, Bao Y, Tian Y, Xia J, Cao D, J Power Sources, **195**, 6463-6467 (2010)
34. Łukaszewski M, Czerwiński A, J Solid State Electrochem, **12**, 1589-1598 (2008)

